Received: 22 June 2018 | Revised: 27 September 2019 | Accepted: 16 October 2019

DOI: 10.1002/stc.2477

RESEARCH ARTICLE

WILEY

Analysis of periodicities in long-term displacement time series in concrete dams

Sonja Gamse[1] | **Maria João Henriques**[2] | **Michael Oberguggenberger**[3] | **Juan Tomé Mata**[4]

[1]Unit for Surveying and Geoinformation, Faculty of Engineering Science, University of Innsbruck, Innsbruck, Austria

[2]National Laboratory for Civil Engineering, Applied Geodesy Division, Lisbon, Portugal

[3]Unit for Engineering Mathematics, Faculty of Engineering Science, University of Innsbruck, Innsbruck, Austria

[4]National Laboratory for Civil Engineering, Concrete Dams Department, Lisbon, Portugal

Correspondence
Sonja Gamse, Unit for Surveying and Geoinformation, Faculty of Engineering Science, University of Innsbruck, Technikerstr. 13, Innsbruck, 6020, Austria.
Email: sonja.gamse@uibk.ac.at

Summary

The hydrostatic-season-time (HST) model is a widely used method in the safety assessment of dams and for the estimation of reversible and irreversible deformations due to different load scenarios. After implementing an optimal HST-model to observational data, the residual time series can still expose some underlying periodicities. In our contribution, the underlying periodicities and their contribution to residual minimisation are further analysed by the Lomb–Scargle normalised periodogram frequency method. The extended HST-model, obtained by adding additional sinusoidal terms for the statistically most significant frequencies, presents a slight statistical improvement on the optimal HST-model. Statistically significant frequencies may not be justified or correlated to some physical process of the dam, but they make it possible to identify a pattern in the analysed period. The analyses are performed for the radial direction of long-term displacement time series measured at the topmost reading station of an inverted pendulum system in the central cantilever of the Alqueva concrete arch dam.

KEYWORDS

concrete arch dam, false alarm probability, hydrostatic-season-time model, Lomb–Scargle normalised periodogram, multiple linear regression

1 | INTRODUCTION

Due to the importance of dams and their potential risk, public legislation regulates safety controls of large dams. The regulations are based on technical guidelines and procedures for the design, construction, and monitoring of dams. The structural safety control of dams is based on monitoring dam behaviour, modelling, and analysing registered observations and engineering interpretation of the results. The response of dams due to the different and varying influences on the structure and its surrounding can be monitored by sensors, such as pendulums, extensometers, inclinometers, rockmeters, fiber optic sensors, and geodetic methods such as levelling, tacheometric observations, and methods of Global Navigation Satellite Systems. On concrete dams, pendulum measurements and geodetic observations in traverse or triangulation networks are usually used to assess horizontal displacements of different elements or parts of the structure.

The advantages of the pendulum system in comparison with the geodetic monitoring systems are higher resolution and precision. The advantage of the geodetic methods is that they can be used to monitor different parts of the dam, that is, dam crests, foundations, abutments, and surrounding areas such as slopes and unstable rock masses along the water reservoir. However, geodetic observations are more expensive; therefore, measurement campaigns are generally

less frequent, usually once or twice a year. With the radical developments in telecommunications, both systems can be easily included in automatic monitoring systems.

For an assessment of the measured displacements, captured by different sensors and methods, a variety of different analysis techniques can be used. The main intention of the dam safety control activity is to compare the actual response of the structure measured by different sensors, with predictions estimated by a mathematical model, with the aim of detecting anomalies early and preventing failures.[1,2] The forces on the dam induce reversible and irreversible deformations. The main phenomena related to the loads that originate the reversible deformations in concrete dams in operation are the reservoir water level and the water and the air temperature variations. Furthermore, the consequences of the changes that occur in the dam body during the lifetime, for example, the swelling, are irreversible deformations. The main three influences can be decomposed using a well-known empirical hydrostatic-season-time (HST) model, described in.[3] The practical implementations of the HST-model are given, for example, in previous studies.[4-7] Further references with the practical implementation of the HST-model are given in Salazar et al.[8]

In many cases, the residual time series can still expose some deterministic pattern after the estimation of an optimal HST-functional model. In order to fulfill the presumption of the regression analysis, that is, for the residuals, it is assumed they have a Gaussian distribution with zero mean and variance σ_ε^2, and are uncorrelated in time domain, and to get a more accurate estimate of unknown parameters of interest and their uncertainties, the periodic errors should be appropriately analysed. In the case of deterministic pattern with underlying periodicities, frequency analysis methods can be implemented to detect possible statistically significant frequencies in residual time series. The functional model can then be extended by sinusoidal functions with estimated frequencies of underlying periodicities. Depending on the type of data, the Fourier transform can be used for the data sets with evenly spaced data,[9] otherwise the Lomb–Scargle normalised periodogram (LSNP),[10] and least squares spectral analysis (LSSA) are proposed in previous studies.[11,12]

The results of previous works involving data from a concrete dam and an embankment dam, in previous studies[4,13] showed that the residuals can still expose small underlying periodicities after implementing an HST-model. The main intent of the presented work is a reevaluation of the HST-model, which is widely used for data analysis of primarily concrete dams due to its simplicity. In this case study, the LSNP is therefore adopted for the periodicity identification in order to examine further—presumed nonannual—frequencies in residual time series after fitting the HST-model to the displacement time series. Here, the measurement data from the Alqueva dam, a concrete arch dam in Portugal, for the time span of 8 years are analysed. For the measurement data of the topmost reading station of the pendulum system that is installed in the central cantilever of the dam, an optimal HST-model is defined for the radial direction. The unknown coefficients of the model are estimated using a multiple linear regression (MLR). In the process of defining an optimal model, the backwards elimination and the parameter selection through the Bayesian Information Criterion (*BIC*) and the Akaike Information Criterion (*AIC*) are used and compared. After defining the optimal HST-model, the residual time series are further analysed for remaining underlying nonannual periodicities using the LSNP frequency method, because the data are captured manually and are nonequidistant. In order to detect and interpret possible correlations with the water level and the temperature, the periodograms were also used to analyse these time series.

The paper is organised as follows. After the introduction, the HST-model, regression analysis, and LSNP frequency method are described in Section 2. In Section 3, the data used are described. In Section 4, the proposed methods are implemented on the data, and the numerical results are interpreted. The conclusions are outlined in Section 5.

2 | MATHEMATICAL BACKGROUND

2.1 | Hydrostatic-season-time model

The HST-model is an empirical model and is based on the previous measurements of the dam response for some period. It was first proposed by Willm and Beaujoint and has since been widely used for data analysis of concrete dams.[14] This and additional models that can be used for analysis of the dam response to external forces, are described in the Swiss Committee on Dams.[3] With the HST-model, three main influences on the dam are modelled:

- the influence of water level in impounding reservoir,
- the influence of air and water temperature, and
- the influence of various processes, whose effects are irreversible or not fully reversible deformations, and may thus accumulate in the lifetime of the dam.

For modelling the water level influence on the displacements, that is, hydrostatic pressure, a polynomial function of up to 4th degree is used:

$$H_i = a_1 \cdot h_i + a_2 \cdot h_i^2 + a_3 \cdot h_i^3 + a_4 \cdot h_i^4, \tag{1}$$

with the relative water level h_i at the epoch t_i: $h_i = \frac{h(t_i)-h_{min}}{h_{max}-h_{min}}$. In Expression (1), $h_{\max}$ and $h_{\min}$ denote a maximal and a minimal water level, respectively, and $h(t_i)$ is a water level for an epoch of observations, t_i, $i = 1, 2, \ldots, N$. The water levels are given in $[m]$.

Thermal effects on the dam behaviour are related to seasonal temperature variations and can be modelled indirectly by a linear combination of sinusoidal functions[3]:

$$S_i = b_1 \cdot \sin(f_a \cdot t_i) + b_2 \cdot \cos(f_a \cdot t_i) + b_3 \cdot \sin^2(f_a \cdot t_i) + b_4 \cdot \sin(f_a \cdot t_i) \cdot \cos(f_a \cdot t_i), \tag{2}$$

with an annual frequency $f_a = \frac{2\Pi}{\triangle t_a}$ and $\triangle t_a = 365,25$ days for the daily data.

For modelling long-term irreversible deformations, strictly monotone functions are proposed.[3] In the case study, the sum of a linear term and a negative exponential function of reduced time, $\tau_i = (t_i - t_1)/(t_N - t_1)$, during the analysed period, $[t_1, t_N]$, is used:

$$T_i = c_1 \cdot \tau_i + c_2 \cdot e^{-\tau_i}. \tag{3}$$

The HST-model can be written for an epoch t_i as:

$$y_i = \hat{y}_i + \varepsilon_i = k + H_i + S_i + T_i + \varepsilon_i, \tag{4}$$

with $\hat{y}_i$ as the model prediction corresponding to the measurement y_i with an error ε_i, and k as an initial constant.

2.2 | Multiple linear regression

The optimal parameters of the HST-model in Equation (4) can be estimated with MLR. The widely used technique of fitting the model to the data is the method of least squares, which minimises the residual sum of the squares, $\sum_{i=1}^{N} \varepsilon_i^2 \rightarrow \min$, where N is the size of measured data. The matrix form of MLR is given as,[15]:

$$\mathbf{y} = \mathbf{X} \cdot \beta + \epsilon, \tag{5}$$

with:

- vector of unknown regression coefficients β_i,

$$\beta_{[k_j \quad \times \quad 1]} = [\ \beta_1 \ \ \beta_2 \ \ \beta_3 \ \ \ldots \ \ \beta_{k_j}\ ]^T,$$

  with the number of included parameters k_j, corresponding to 11 unknown parameters of the HST-model, k, $a_1 - a_4$, $b_1 - b_4$, $c_1 - c_2$ (Equation 4),
- vector of dependent variables,

$$\mathbf{y}_{[N \quad \times \quad 1]} = [\ y_1 \ \ y_2 \ \ y_3 \ \ \ldots \ \ y_N\ ]^T,$$

  in the HST-model corresponding to measured displacements,
- vector of residuals, and

$$\epsilon_{[N \quad \times \quad 1]} = [\ \varepsilon_1 \ \ \varepsilon_2 \ \ \varepsilon_3 \ \ \ldots \ \ \varepsilon_N\ ]^T,$$

- design matrix or matrix of the levels of the k_j regressor variables,

$$\mathbf{X}_{[N \quad \times \quad k_j]} = \begin{bmatrix} x_{11} & x_{12} & x_{13} & \ldots & x_{1k_j} \\ x_{21} & x_{22} & x_{23} & \ldots & x_{2k_j} \\ \vdots & \vdots & \vdots & \ldots & \vdots \\ x_{N1} & x_{N2} & x_{N3} & \ldots & x_{Nk_j} \end{bmatrix}.$$

In order to keep the model as robust to outliers as possible and to avoid the problem of multicollinearity between the variables, an optimal model should be defined within a set of all possible models of the statistical model class chosen for a specific case study. The statistical parameters, such as the multiple coefficient of determination, R^2, and residual

mean square error, *MSE*, and its root value, *RMSE*, often select a model candidate with more free parameters than an optimal one, which can lead to a model with (strongly) correlated variables. Multicollinearity can cause difficulties in the proper specification and the effective estimation of the structural relationship type.[16] Furthermore, significant residuals or significant influences can be overlooked, because the identified model depends too much on the data, in which the noise is present.[15] The well-known *AIC* and *BIC* methods for parameter selection with penalty terms against overparametrisation can be used for model ranking.* The methods present a more objective attempt than a backwards elimination because the significance of each parameter depends strongly on the set of included parameters. The formulas used in the computations (Section 4) are given in Yuen et al.[18] and are modifications of the original formulas proposed in Schwarz[19] and Akaike.[20] The optimal model is defined by maximizing the objective function *AIC* over model candidates $C_j, j = 1, 2, \ldots, N_C$:

$$AIC(C_j) = \ln L_j - k_j, \tag{6}$$

or the objective function *BIC*:

$$BIC(C_j) = \ln L_j - \frac{1}{2} \cdot k_j \cdot \ln N, \tag{7}$$

with k_j the number of parameters included in j-th model and the likelihood function L_j of the model C_j:

$$L_j = (2 \cdot \pi)^{-N/2} \cdot \sigma_\varepsilon^{-N} \cdot \exp\left[-\frac{N}{2 \cdot \sigma_\varepsilon} \cdot J_g\right], \tag{8}$$

where J_g is the goodness-of-fit function:

$$J_g = \frac{1}{N} \cdot \sum_{i=1}^{N} \left[y_i - \sum_{j=1}^{k_j} x_{ij} \cdot \beta_j \right]^2. \tag{9}$$

For residuals, it is assumed they have a Gaussian distribution with zero mean and variance σ_ε^2, $\varepsilon_i \sim N(0, \sigma_\varepsilon^2)$ and are uncorrelated, $\sigma(\varepsilon_i, \varepsilon_j) = 0 \; \forall i, j \ni i \neq j$.

2.3 | Lomb–Scargle normalised periodogram frequency method

After defining the optimal HST-model, the residual time series can be further analysed for possible remaining underlying periodicities, which should be analysed and extracted in order to get a reliable estimate of unknown parameters in the HST-model and their uncertainties. The underlying periodicities can be compensated by the inclusion of additional sinusoidal terms of significant frequencies into the model.

Spectral analysis or frequency domain analysis provides an alternative way of interpreting the underlying process of the time series and can be a useful tool for some applications. It enables the estimation of unknown significant periodicities in time series of different measurements, to extract natural frequencies, to analyse similarities in response of different parts of a structure, and to estimate possible correlations between measured influences and measured responses of a structure.

In order to identify periodic effects, frequency methods are usually used. In frequency analysis, two cases should be distinguished—time series with a constant time sampling and time series with unequally spaced data and data gaps present. In the first case, the Fourier transform (FT) can be used.[9] Otherwise, the frequency methods such as LSSA and LSNP are proposed. The frequency methods are for example very popular for analysing periodic signals in GPS/GNSS time series for geodynamic purposes or structural monitoring. The influence of local environmental effects such as rain, temperature, or earth crust load on the coordinate time series of selected IGS (International GNSS Service) stations was analysed by continuous wavelet transform signal reconstruction.[21] The residual time series after adopting a site motion model, which is used on the time series of permanent GPS/GNSS stations for analysing crustal deformations and other geophysical phenomena of plate tectonics, were analysed for underlying periodicities by LSSA in Nobakht et al.[22] In Erol,[23] the LSSA was used on time series captured by inclination sensors and GPS data for continuous monitoring of a tall building in order to detect natural frequencies and possible anomalies. In Zhang et al.,[24] the authors adopted a fast FT algorithm for detecting the local dominant frequencies of two sets of GNSS real bridge data. In Pytharouli and Stiros,[25]

*The adjusted R^2 statistic, $R^2_{adj,k_j} = 1 - (N-1)/(N-k_j) \cdot (1 - R^2_{k_j})$, k_j is a fixed number of variables, Montgomery et al.,[17] is another simple statistical indicator that takes the number of model parameters into account, but for $N \gg k_j$, as in our case, $R^2_{adj,k_j} \approx R^2_{k_j}$.

discrete FT (here, a 3rd-order polynomial fitting and a moving window of four observations were used for data interpolation) and Lomb normalised peridogram were adopted to examine whether the geodetically captured displacement time series of monitoring points on the crest of a concrete dam containing periodic signal/s and its/their correlation with the water level fluctuations. Both methods were compared with trigonometric-polynomial fitting. The results confirmed the capability of spectral analysis techniques, especially of the Lomb normalised periodogram for analysing nonequidistant data, for detecting a dominant annual period even in very infrequently spaced data: two surveying campaigns per year on average. In continuation of this work,[26] the authors compared the results of Lomb normalised peridogram with LSSA, and introduced also some further case studies such as analysing geodetic observations of ground deformation (convergence) during the tunnel excavation.

In continuation, we summarise the LSNP, which will be adopted in the presented case study. The LSNP algorithm was developed by Lomb[10] and Scargle.[27] The algorithm is proposed for spectral analysis of evenly or unevenly spaced data. A set of observations, $\{y_i = y(t_i), i = 1, 2, \ldots, N\}$ is modelled as[10,28]:

$$y_f(t_i) = a_L \cdot \cos(\omega \cdot (t_i - \tau)) + b_L \cdot \sin(\omega \cdot (t_i - \tau)),^{\dagger} \tag{10}$$

where the periodogram at the frequency f is estimated as,[27]:

$$P_y(f) = \frac{1}{2 \cdot \sigma^2} \left(\frac{\left[\sum_i (y_i - \bar{y}) \cdot \cos(\omega \cdot (t_i - \tau))\right]^2}{\sum_i \cos^2(\omega \cdot (t_i - \tau))} + \frac{\left[\sum_i (y_i - \bar{y}) \cdot \sin(\omega \cdot (t_i - \tau))\right]^2}{\sum_i \sin^2(\omega \cdot (t_i - \tau))} \right), \tag{11}$$

where ω is the angular frequency, $\omega = 2\pi f$, and $\bar{y}$ and σ^2 are the mean and variance of the measurements. Time delay τ is defined by the inverse of the tangent function:

$$\tan(2\omega\tau) = \frac{\sum_i \sin(2 \cdot \omega \cdot t_i)}{\sum_i \cos(2 \cdot \omega \cdot t_i)}. \tag{12}$$

After computing the LSNP, the assessment of statistical significance of periodogram peaks is performed. Namely, the data quality and quantity are reflected directly in the height of the peak in relation to the background noise. The typical approach to quantify the significance of a peak in the spectrum $P_y(f)$ is the False Alarm Probability (FAP), which measures the probability that a dataset with no signal (noise only) would lead to a peak of a similar magnitude. Previous studies[27,29] showed that the power at a given frequency $P_y(f)$ follows an exponential probability distribution in the case of the null hypothesis: the data is composed of independent Gaussian random variables. The statistical significance of a frequency power peak can be computed as follows. Denoting the height of the LSNP at a preselected frequency f as $z = P_y(f)$, the probability distribution of a power peak z is given by $Pr(z) = e^{-z}$, with the cumulative probability of observing a periodogram value less than z, in data with no periodic signal[27,29]:

$$F(z) = 1 - e^{-z}. \tag{13}$$

The interest is the distribution of the highest peak of the periodogram.[29] Considering the maximum value of the periodogram, $z = \max_M P_y(f)$, and statistical penalty for inspecting a large number of frequencies, the probability that none of M independent frequencies, $f_1, f_2, \ldots, f_M$, give values $P_y(f_1), P_y(f_2), \ldots, P_y(f_M)$ larger than z is $(1 - e^{-z})^M$, the FAP of the null hypothesis, that is, the significance level of any peak z in $P_y(f)$ is[27,30]:

$$p = FAP(z) = 1 - (1 - e^{-z})^M. \tag{14}$$

The power level limit, z_0, for a chosen value of p (significance level) is computed as:

$$z_0 = -\ln(1 - (1 - p)^{\frac{1}{M}}). \tag{15}$$

z_0 presents the power spectral density level above which the detected frequency power is statistically significant with $(1 - p)$-confidence level. A low probability value p indicates a high degree of power peak significance in the associated periodic signal. Further possibilities of computing FAP are discussed in Baluev[31] and Zhou and Sornette.[32]

[†] $y(t_i)$ denotes an observation at time step t_i and $y_f(t_i)$ its corresponding estimated value modelled by cosine terms of some frequencies. Their relation can be written as follows: $y(t_i) = y_f(t_i) + \varepsilon_i$.

In the presented case study, the LSNP is iteratively adopted on different data sets in order to examine also nonannual periodicities: on direct displacement observations in the first step and subsequently on residual time series after adopting the optimal HST-model and its extended form. In each iteration step, we have a new data set (i.e., direct observations or residuals after adopting some model) and the periodograms expose different scatter of frequencies, which are tested for their significance by the FAP test. In order to analyse possible correlations of nonannual periodicities with the water level and the temperature, the LSNP was computed also for these time series.

3 | CASE STUDY: ALQUEVA CONCRETE ARCH DAM

In the numerical evaluations, the measured data which are part of the monitoring system on the Alqueva dam are processed and analysed. The dam is located on the Guadiana River and is designed as a multipurpose dam for irrigation, water supply, electric power generation, and outdoor activities in the Alentejo region, in south Portugal. The main structure is a concrete arch dam, with a maximum height of 154 m, measured from the foundation bottom, and a crest length of 458 m. Its hydrological basin has an area of $55,000\ km^2$. The dam was built between 1998 and 2002. The first filling of the reservoir began in February 2002. In January 2010, the lake was filled to the planned level (full storage water level at an elevation 152 m, Figure 2), with a reservoir surface area of 250 km^2.[33]

The installation of monitoring equipment and formulation of the safety control procedures of the main structure were carried out during the construction, according to the monitoring plan.[34] The monitoring plan also includes safety procedures to be followed during different periods of the dam maintenance, according to the Portuguese regulations.[35] The plan was complemented by different technical plans, including one with requirements for geodetic monitoring of the dam.[33,36-38]

3.1 | Measurements

Eight inverted pendulums have been installed in the dam body (Figure 1), to measure horizontal displacements. Each inverted pendulum system consists of a stainless steel wire anchored in the stiff rock beneath the structure, with a float fixed at its upper end. The absolute internal lateral displacements at several reading stations located along the steel wire in inspection galleries are measured in the radial (orthogonal to the downstream face of the block) and tangential (parallel to the downstream face) direction. Sensor readings are done manually, with weekly periodicity in the first years (2000–2004), which were reduced to one or two readings per month after 2005. In the paper, the measured data for radial direction at the topmost reading station, 17, of the pendulum FP4 installed in the central cantilever (middle of the dam, at the height 148.25 m) are analysed. The displacement variations in tangential direction are near zero and lie within measurement uncertainties, in the range $\pm 1\ mm$ for all pendulum reading stations. In order to perform the evaluations independently from different time spans of the registered data, the analyses are done for the period of 8 years, between January 1, 2004, and November 31, 2011. For this period, all of the measured values are available, and at the end of year 2003, the water level reached the height of the topmost reading station of the central pendulum, FP4-17 (Figure 2), which remains below the water level for the whole period of data available. The period before December 4, 2003, presents the first filling of a reservoir and should be analysed separately,

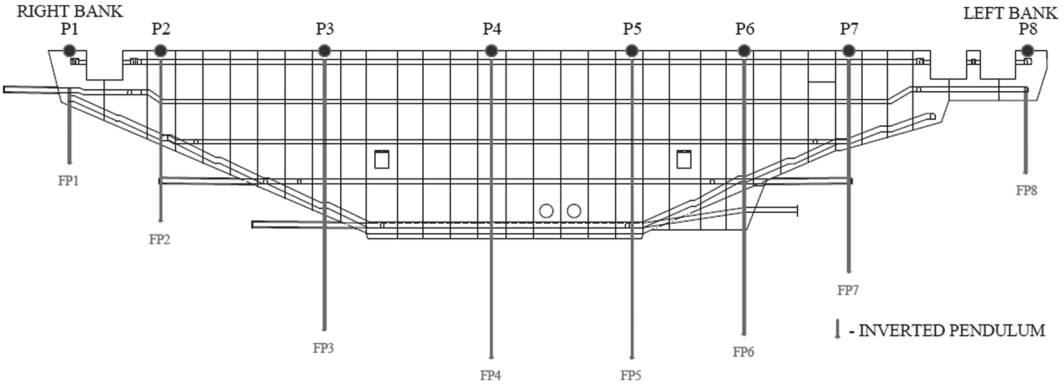

FIGURE 1 Pendulum systems with horizontal inspection galleries

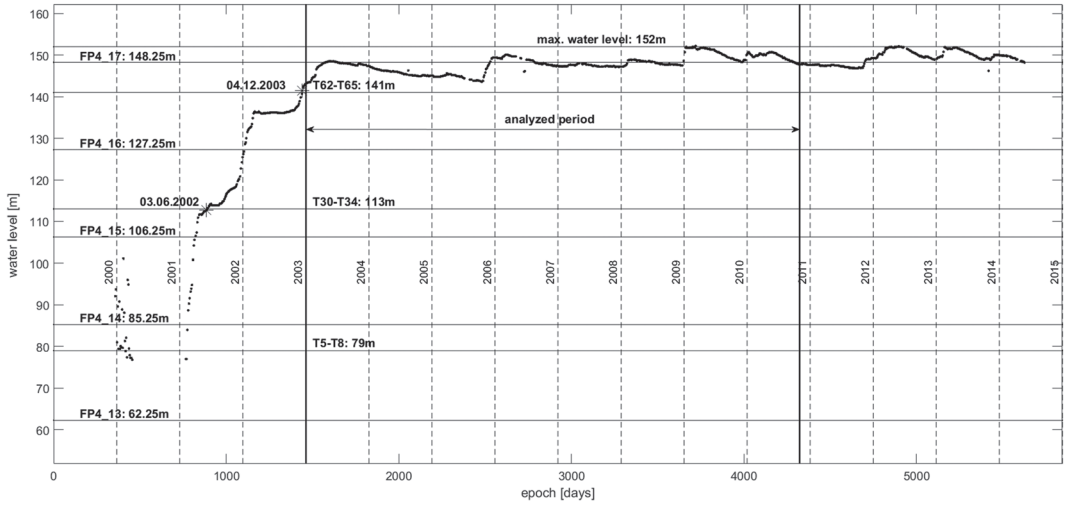

FIGURE 2 Water level with position of pendulum reading stations and temperature sensors and planed (maximum) water level

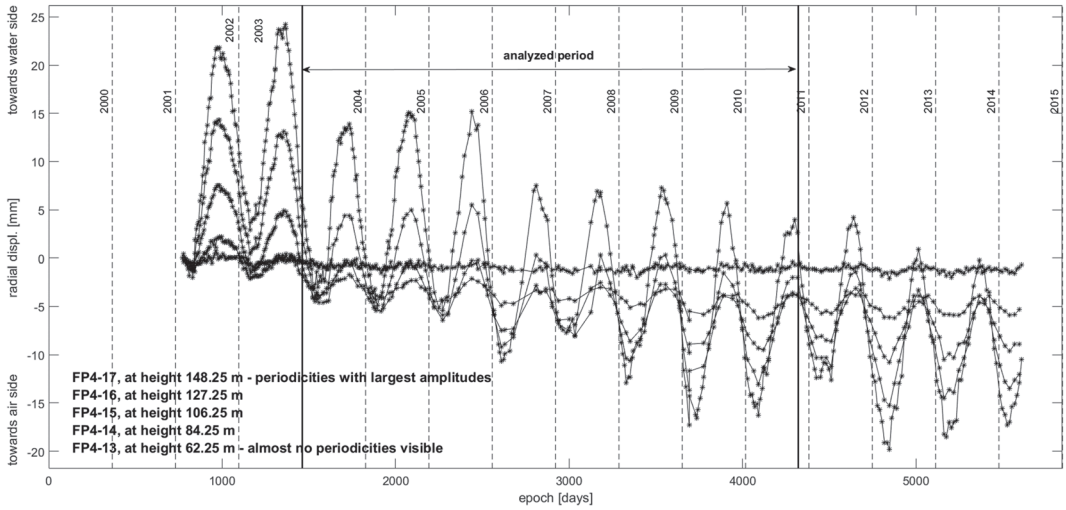

FIGURE 3 Radial displacements in [*mm*] for five reading stations along the pendulum FP4

which is not the scope of presented work. In the analyses, the time series of following manually captured values are included:

- readings in the radial direction at the topmost reading station of the pendulum in the central cantilever, FP4-17 (Figure 3),
- readings at the temperature sensors T30-T34 at the height 113 *m*: T30 and T31 are installed on the water side, T32 approximately in the middle, and T33 and T34 on the air side of the dam structure; readings at the central temperature sensor, T32, are done with higher frequency, (Figure 4),
- readings at the temperature sensors T62-T66 at the height 141 *m*: T62 and T63 are installed on the water side, T64 approximately in the middle, and T65 and T66 on the air side of the dam structure; readings at the central temperature sensor, T64, are done with higher frequency (Figure 5),
- readings of the air temperature at the meteorological station located near the dam, with the data up to November 31, 2011, and after July 1, 2014 (Figures 4 and 5), and
- readings of the water level in impounding reservoir (Figure 2).

The temperature readings are not directly modelled in the HST-model. In this case study, they are used to analyse potential correlations of periodicities in residual time series of the HST-model with the frequencies in temperature time series and for the interpretation of the first.

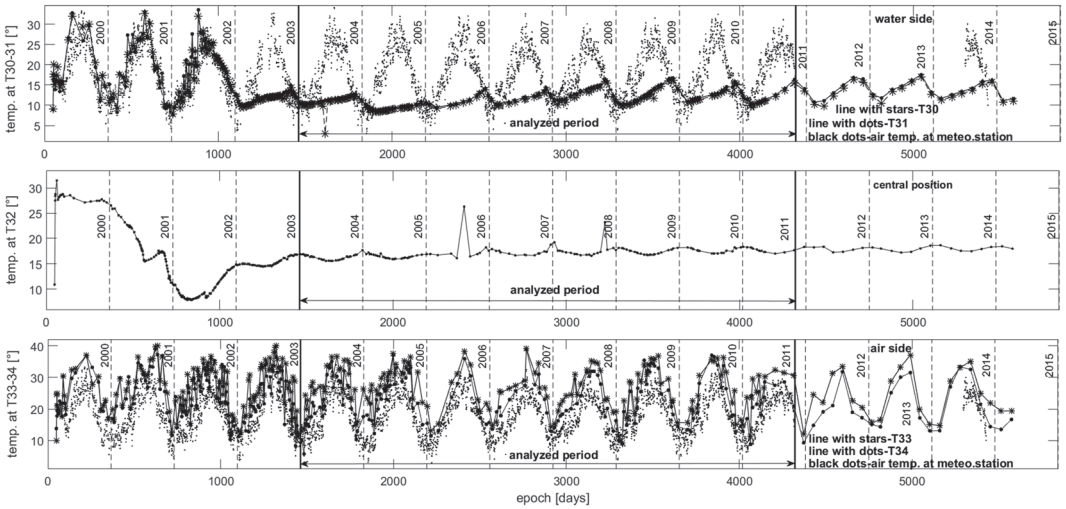

FIGURE 4 Temperatures measured at sensors T30-T34, at the height 113 m, and air temperature measured at meteorological station (black dots)

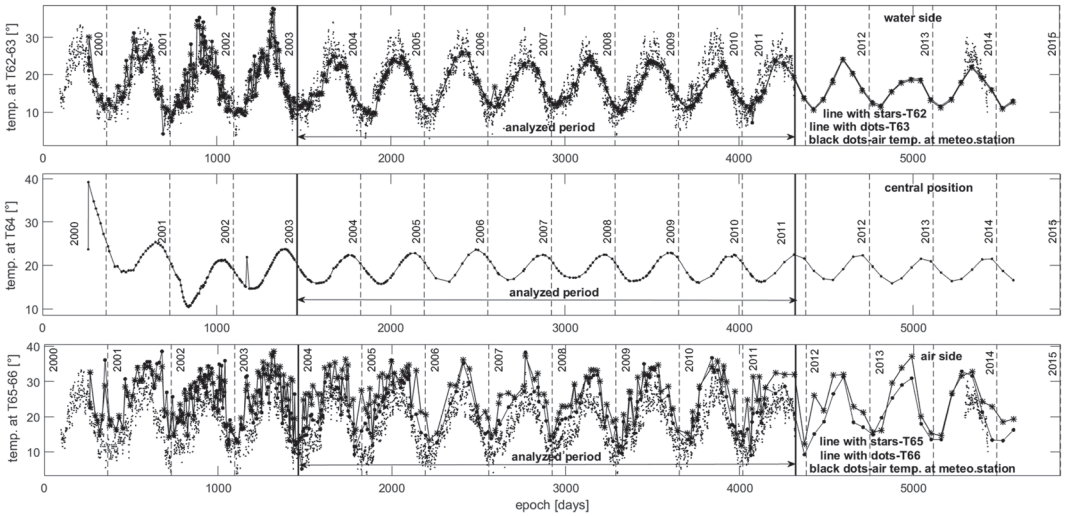

FIGURE 5 Temperatures measured at sensors T62–T66, at the height 141 m, and air temperature measured at meteorological station (black dots)

4 | NUMERICAL ANALYSES AND RESULTS

4.1 | Model selection

The main intent of this work is to analyse the frequencies of the remaining periodic signal in the residual time series, their statistical significance, and the contribution of the additional sinusoidal terms in the optimal HST-model to the reduction of residuals. In order to perform analyses and interpretation based on a representative time period, the data for the periods January 2004 and October 2011 were analysed. Namely, the water level reaches the elevation of temperature sensors T62–T66 at the end of the year 2003, which remain below the operating water level afterwards. After the year 2011, the data of the air temperature at the meteorological station are not registered continuously.

The optimal HST-model for the prediction of radial displacements in the FP4-17 (at the height 148.25 m) was first defined by the iterative backwards elimination of statistically nonsignificant parameters (c_1, b_3, a_1), where a test statistic for hypothesis testing of estimated regression coefficients, given in Montgomery et al.[17] and used for a case study of an embankment dam in Gamse and Oberguggenberger,[4] for a 95% confidence level was used. The selection of parameters was checked by the *BIC* and *AIC* classification, where the HST-model with the statistically significant parameters k, a_2, a_3, a_4, b_1, b_2, b_4, and c_2 was the 8th and 3rd topmost model within $N_C = 2^{(11-1)} - 1 = 1023$ model candidates. The constant

TABLE 1 Parameter values with standard deviations, [mm], of the optimal HST-model for the prediction of radial displacements in the FP4-17 (at the height 148.25 m); parameters a_1, b_3 and c_1 are estimated as statistically non-significant

	k, σ	a_1, σ	a_2, σ	a_3, σ	a_4, σ	b_1, σ	b_2, σ	b_3, σ	b_4, σ	c_1, σ	c_2, σ
parameter [mm]	−7.065		−37.831	59.988	−30.307	−8.388	−3.521		−0.560		16.655
stan.deviation [mm]	0.419		5.401	12.849	7.869	0.101	0.098		0.096		0.438

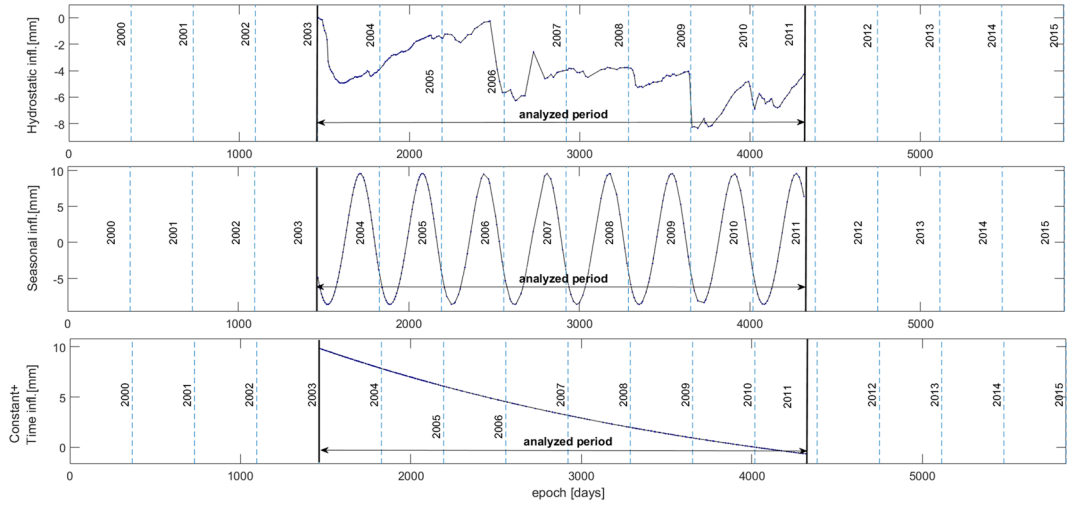

FIGURE 6 Hydrostatic, seasonal and time influence estimated by the optimal hydrostatic-season-time-model for the prediction of radial displacements in the FP4-17 (at the height 148.25 m)

term is included in all of the model classes, and the remaining 10 parameters ($a_1 - a_4$, $b_1 - b_4$, $c_1 - c_2$) constitute the model class candidates. The R^2 and $RMSE$ values are 0.99 and 0.99 mm, respectively. The parameter values with standard deviations for the optimal HST-model are given in Table 1. The seasonal term involves three parameters, b_1, b_2, and b_4, for indirect modelling of the temperature influence on the dam. The hydrostatic influence is modeled by the a_2, a_3 and a_4 parameters. For the time component, the negative exponential function exposes much stronger significance than the linear term, with p-values for the corresponding coefficients $p(c_1) = 0.93$ and $p(c_2) = 2.73 \cdot 10^{-7}$, which indicates a good tendency of stabilisation of long-term displacements with time and coincides with the expectation from the visual estimation of displacements in Figure 3.

The estimated parameters constitute model regressors which enable the computation of hydrostatic, seasonal, and time influence (Figure 6). The amplitude of the seasonal term amounts to 9.06 mm for the period 2004 − 2011.

4.2 | Displacement and residual time series analysis using Lomb–Scargle normalised periodogram

In finding observations (in our case measured deformations) that are outliers for the estimated model, the residuals are tested to a limit bound d, as proposed in[3]:

$$|\varepsilon_i| = |y_i - \hat{y}_i| < d. \tag{16}$$

If the difference is bigger than d, the value y_i is identified as unexpected and demands an analysis of the possible reasons of discrepancy. The value d is usually a multiple of the reference standard deviation $\hat{\sigma}$, computed for some reference, calibration period[3,39,40]:

$$\hat{\sigma} = \sqrt{(\varepsilon_1^2 + \varepsilon_2^2 + \ldots \varepsilon_N^2)/(N - k_j)}. \tag{17}$$

The limit bound for analysed data amounts to $d = \hat{\sigma} = 1.01$ mm. The residuals with d- and $2 \cdot d$-limit bound for the optimal HST-model are plotted in Figure 7. The reason for a larger outlier in year 2007 lies most probably in the measured water level (Figure 2). The residual plot and autocorrelation of residuals (Figure 8) indicate underlying periodicity(ies) and time correlation of residuals.

The main intent of the work is to analyse the remaining systematic pattern. Namely, the basic assumption of the statistical regression model is a zero mean error $\boldsymbol{\varepsilon}$ with a constant variance σ_ε^2 and uncorrelated components, $\sigma(\varepsilon_i, \varepsilon_j) = 0$ $\forall i, j \ni i \neq j$, with a normal distribution, $\varepsilon_i \sim N(0, \sigma_\varepsilon^2)$. A frequency analysis was adopted for estimating the unknown fre-

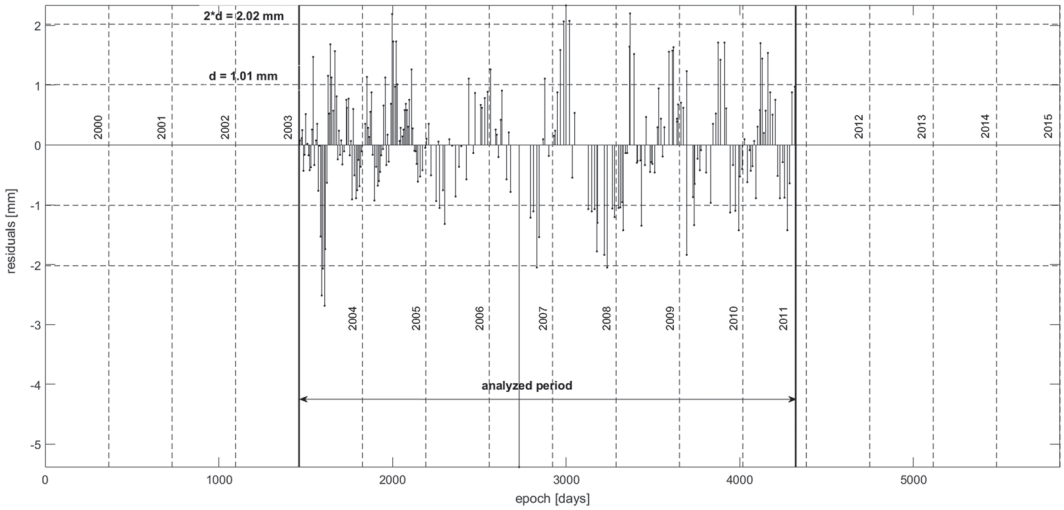

FIGURE 7 Residuals for the optimal HST-model for the prediction of radial displacements in the FP4-17 (at the height 148.25 m), with d- and $2 \cdot d$-limit bound

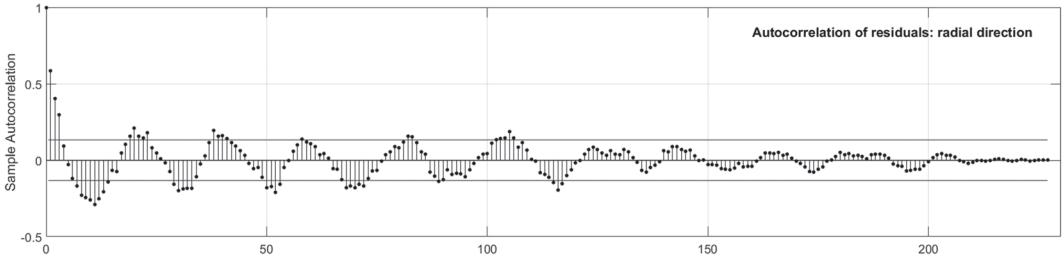

FIGURE 8 Autocorrelation of residuals for the optimal HST-model for the prediction of radial displacements in the FP4-17 (at the height 148.25 m)

quencies of underlying periodicities and their statistical significance. Due to the fact that the data are unevenly spaced, the LSNP frequency method is used. By iteratively adding additional sinusoidal terms of significant frequencies into the optimal HST-model, the deterministic signal is separated from the residual time series and remaining errors should tend to a random distribution.

First, it is necessary to define the frequency limits and the grid spacing of the periodogram. The frequency limit on the low end for a set of observations spanning a length of time $T = t_{max} - t_{min}$ can be chosen as $f_{min} = 1/T$; in our case $T = 2850$ days. The minimum frequency f_{min} completes one oscillation cycle. Often, it is more convenient to set the minimum frequency to zero, as it does not add much of a computational burden and is unlikely to add any significant spurious peak to the periodogram. The high-frequency limit is more interesting. In order to not miss relevant information, it is important to compute the periodogram up to some well-motivated limiting frequency f_{max}.[29] In our case, the upper limit is based on the Nyquist limit, which is defined by the temporal resolution. The upper limit to the Nyquist frequency, f_N, for the observations that are separated by integer multiples of some underlying time-unit δ_* can be written as[41]:

$$f_{max} = f_N = 0.5/\delta_* = 0.5 \cdot f_s. \tag{18}$$

The sampling rate in a frequency domain, f_s, of a discrete signal is in our case $f_s = (1cycle)/(1day)$, with $\delta_* = 1\ day$ as the minimal temporal resolution. The periodogram exposes symmetry above the Nyquist frequency.

Furthermore, an appropriate oversampling interval or frequency grid has to be chosen for the periodogram to successfully detect all statistically significant frequencies in the predefined frequency range. Too coarse a grid can lead to a periodogram that entirely misses the relevant peaks. To ensure that the grid sufficiently samples each peak, it is prudent to oversample by some factor n_0 and use a frequency grid of size $\triangle f = 1/(no \cdot T)$. But if too fine a grid is chosen, it can lead to unnecessarily long computation times. The number of required periodogram evaluations is $N_{eval} = n_0 \cdot T \cdot f_{max}$. The values n_0 ranging from $n_0 = 4$ to $n_0 = 10$ are suggested.[29,30] For periodograms computed and discussed in this con-

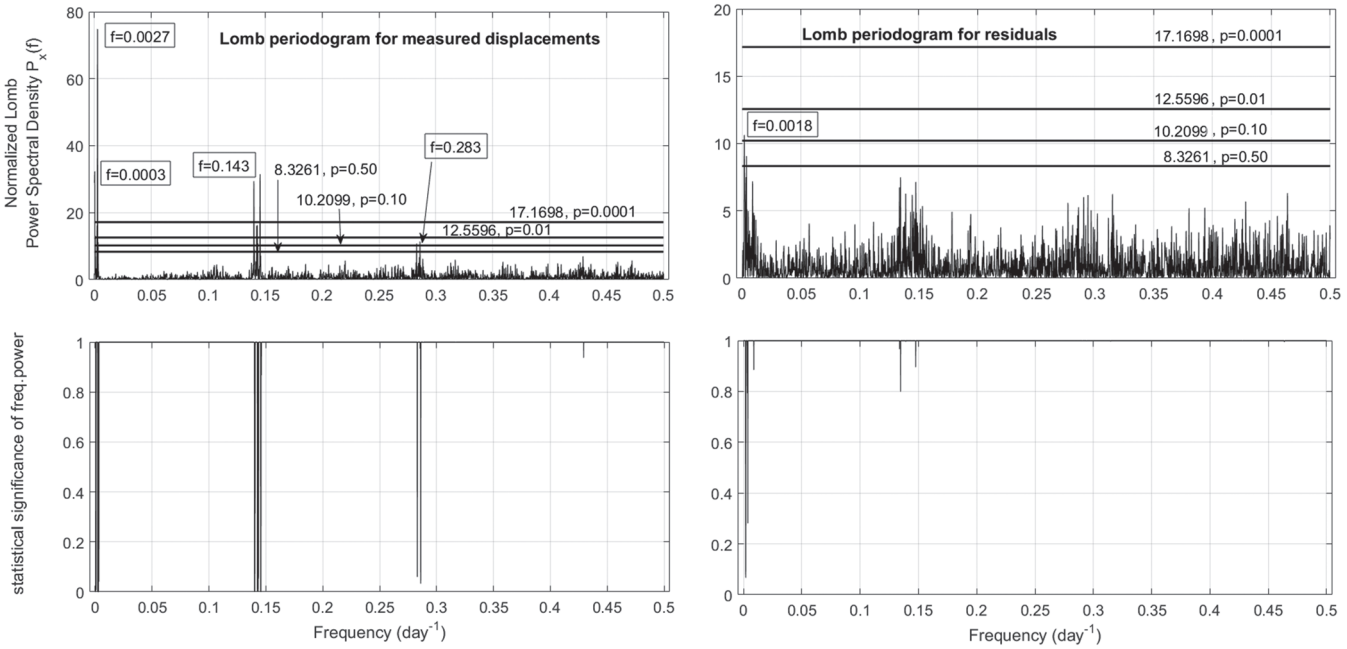

FIGURE 9 Top: Lomb–Scargle normalised periodogram with power level limits, z_0, corresponding significance levels $p = .50, .10, .01,$ and $.0001$. Below: probability distribution of frequency power; for measured displacements (left) and for residuals of the optimal HST-model (right)

tribution, the sampling factor $n_0 = 10$ is used. Tests with different values of the sampling factor n_0 were done, also larger than 10. The computations confirmed that a larger value of the sampling factor does not contribute significantly to the precision of frequency detection.

After computing the LSNP on displacement time series and residual time series of the optimal HST-model, for the defined frequency limits and grid spacing, the periodogram peaks are analysed for their statistical significance as described in Subsection 2.3. In Figure 9, the normalised Lomb–Scargle power spectral density periodogram, $P_y(f)$, and diagram of the statistical significance of frequency power are plotted for frequency range $[0, f_N]$ and sampling factor $n_0 = 10$. The FAP thresholds correspond to the confidence level $(1 - p)\%$ of $50, 90, 99, 99.99\%$ (i.e. ,$p = .50, .10, .01,$ and $.0001$ significance level) and the number of computed frequencies $M = N_{eval}$. For displacement time series, the frequencies 0.0027, 0.143 per day, and an additional low frequency 0.0003 per day, corresponding to the period 370 days (approximately annual period), 7 days, and 9.1 years, prevail as statistically most significant, with the 99.99% confidence level. The frequency 0.283 per day (corresponding to 3.5 days) was detected at 90%-confidence level. After adopting the optimal HST-model, where the model incorporates parameters of the sinusoidal term with annual pulsation (Subsection 4.1), which is also detected and confirmed as the most significant by adopting the LSNP on displacement time series, the LSNP is used to further analyse underlying periodicities in residual time series. The power spectrum of residual time series detects in two iterative steps low frequencies of 0.0018 and 0.0023 per day, corresponding to the period 1.5 and 1.2 years, as significant with the 90%- and 99%-confidence level respectively.

4.3 | Interpretation of frequencies and analysis of temperature variations

In Figures 10, 11, 12, and 13, the LSNP of measured water level, air temperature, and temperatures measured at sensors T30–T34 and T62–T66 are plotted. The statistically most significant frequency, that is, annual frequency, in coordinate time series, corresponding to the 99.99% confidence level ($p = .0001$), is justified by a strong temperature influence on concrete arch dams, with the annual pulsation of air temperature, which is strongly correlated to measured temperatures in the dam (Figures 4 and 5). The second statistically most significant frequency, which is detected in displacement time series, that is, 0.143 per day, corresponding to the period 7 days, is detected in all time series except in time series of the air temperature. The frequency spike indicates the time interval that appears most frequently in unevenly spaced data (Figure 14). Also in the literature, it is reported that the LSNP detects frequency spikes, which correspond to the most frequent time intervals of measurements in unevenly spaced data, as statistically significant.[29]

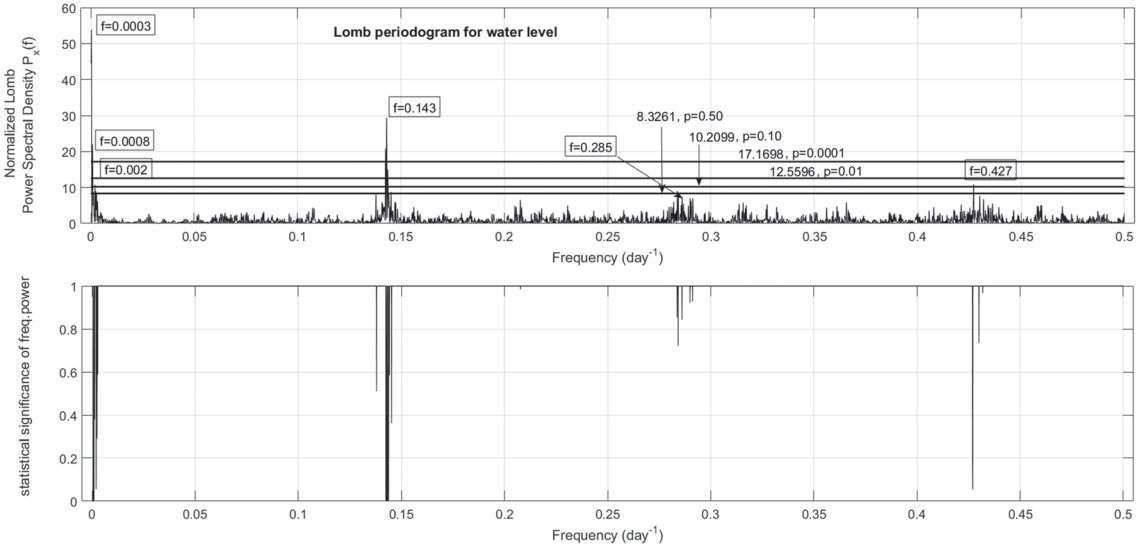

FIGURE 10 Lomb–Scargle normalised periodogram of water level with statistical significance

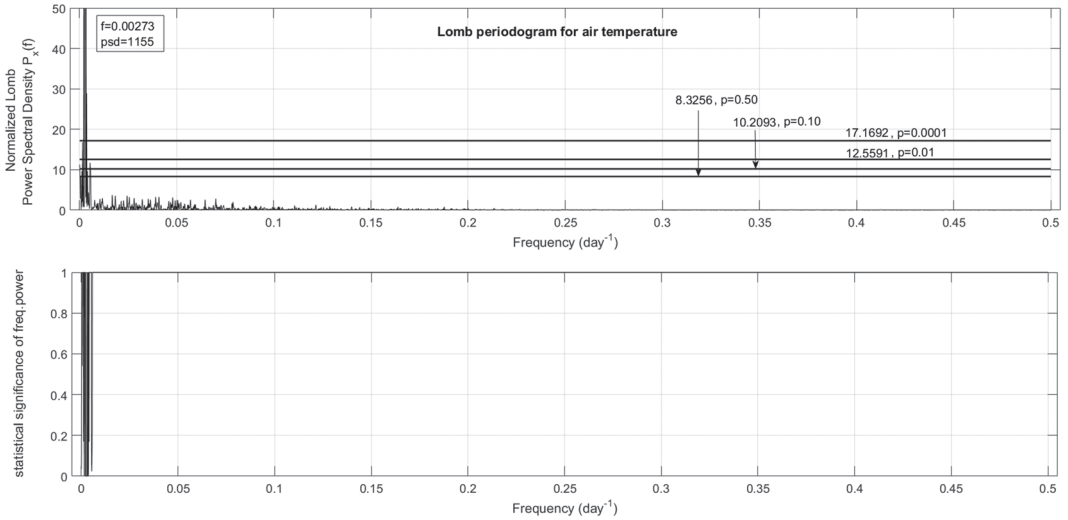

FIGURE 11 Lomb–Scargle normalised periodogram of air temperature with statistical significance

After adopting the optimal HST-model, where the periodical thermal effects are modeled by incorporating the parameters b_1, b_2, and b_4, the LSNP is used in an iterative manner to further analyse possible underlying periodicities in residual time series. The power spectrum of residual time series detects a low frequency of 0.0018 per day, corresponding to the period 1.5 years, as significant at the 90% confidence level, and a low frequency of 0.0023 per day, corresponding to the period 1.2 years, as significant at the 99% confidence level, in the first and second iteration, respectively. The estimated frequencies are valid within the time period of modelling and were not detected in the time series of measured displacements (Figure 9). After an iterative inclusion of these frequencies into the optimal HST-model, the metrics R^2, *RMSE*, signal-to-noise ratio *SNR*, and percentage of their improvement, of the extended HST-model expose slight improvement (Table 2). Furthermore, the autocorrelation of residuals for the extended HST-model is plotted in Figure 15 and shows a lower correlation of residuals in the time domain. After two iterations, 18 lags lie outside the 95%-confidence bound, whereas for the optimal model 46 lags fall outside. Namely, the confidence bound enclose those lags for which the null hypothesis, that is, the data are randomly distributed, is assumed to hold.

The frequencies, which are detected in the displacement frequency power spectrum as significant with a lower confidence level (Figure 9) do not reach the threshold for $p = .50$ in the frequency power spectrum of residual time series.

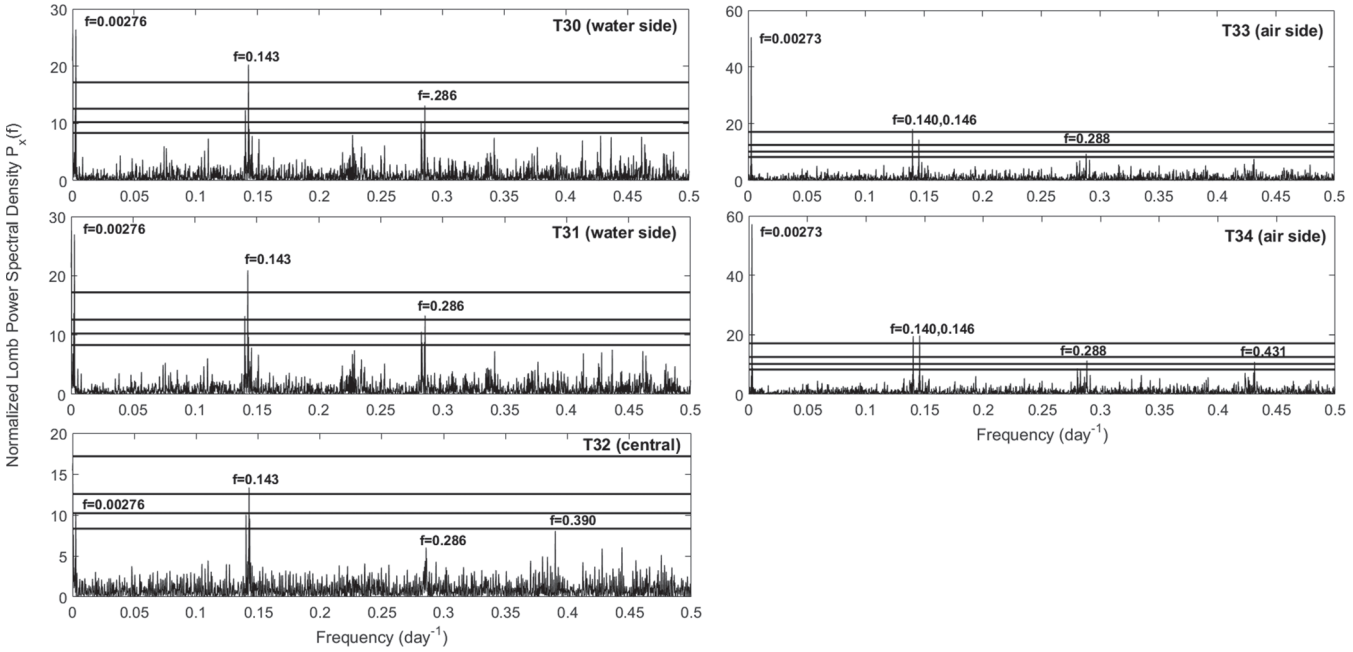

FIGURE 12 Lomb–Scargle normalised periodogram of temperature sensors T30–T34 at the height 113 m, with $p = .50, .10, .01,$ and .0001 significance levels (from lowest to the top)

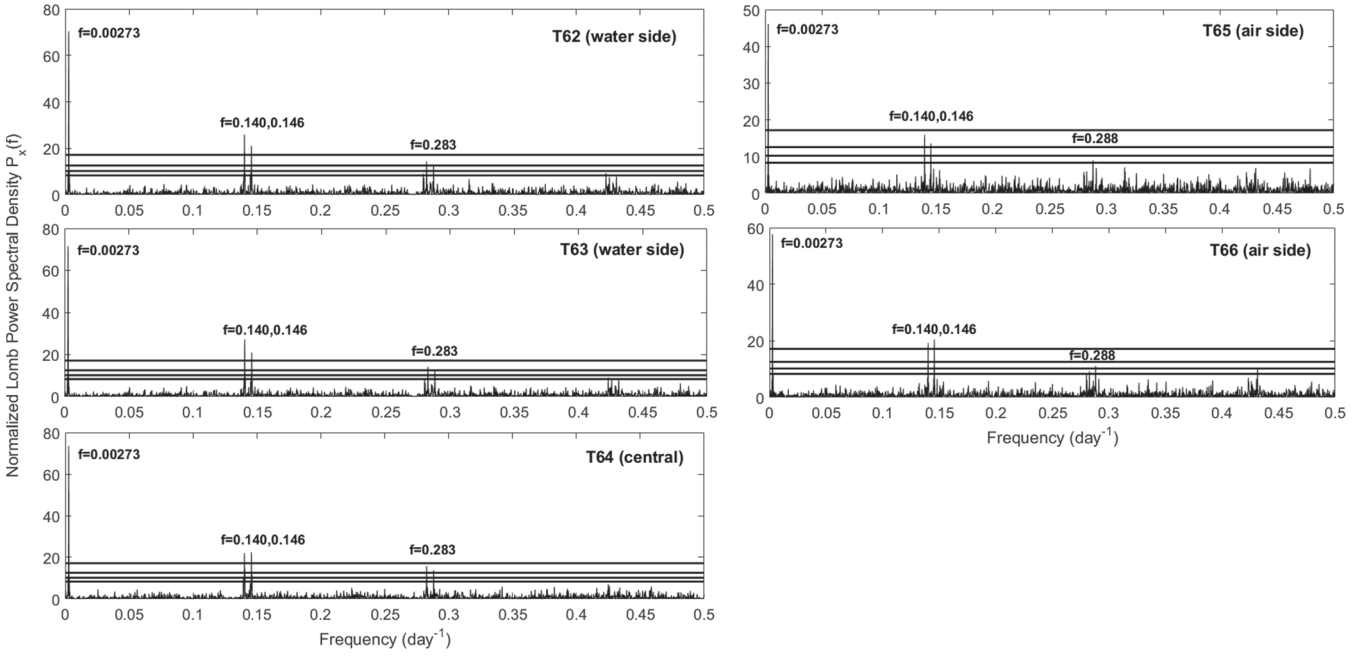

FIGURE 13 Lomb–Scargle normalised periodogram of temperature sensors T62–T66 at the height 141 m, with $p = .50, .10, .01, and .0001$ significance levels (from lowest to the top)

The optimal HST-model includes parameters k, a_2, a_3, a_4, b_1, b_2, b_4, and c_2. The extended model in the 1st iteration is obtained by adding sine and cosine terms with the frequency f_1 to the optimal HST-model, and in the 2nd iteration, additional sine and cosine term with the frequency f_2 are added to the extended model of the 1st iteration.

From the graphical presentation of displacements estimated by the optimal HST-model and estimated displacements after the model extension (Figure 16), it can be seen that the extended model slightly improves the modelling of peaks. Changes in annual amplitudes after adopting the extended HST-model are plotted in Figure 17. It is expected that both models—the optimal one and the extended—will expose a similar trend with slight deviations at annual peak amplitudes also for the prediction, which can be seen in Figure 18.

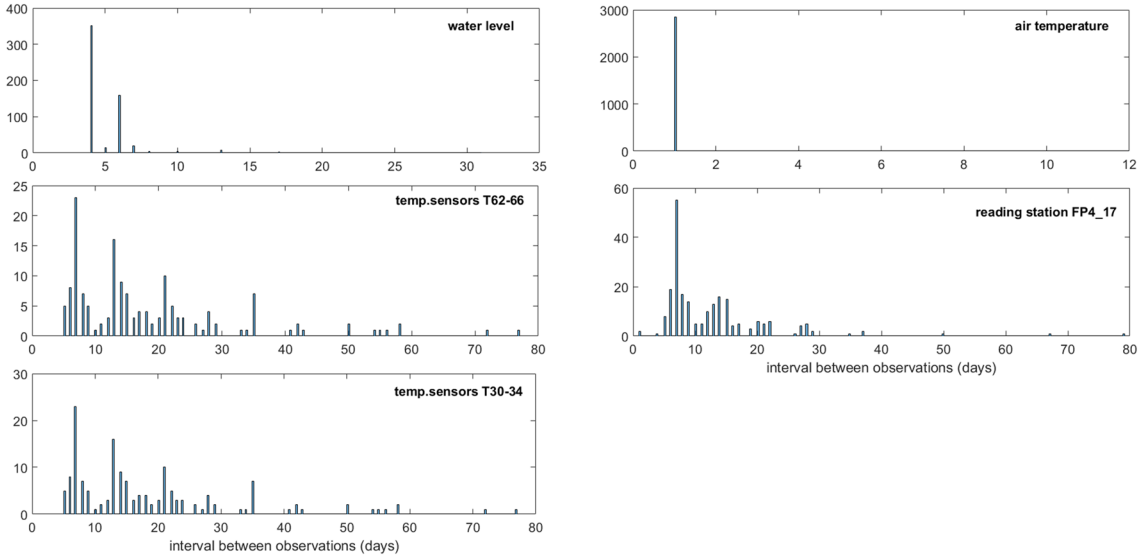

FIGURE 14 Histograms of measurement intervals

TABLE 2 Metrics R^2, *RMSE* and *SNR*, with the percentage of their improvement, for the optimal HST-model and the extended HST-model after iterative inclusion of sinusoidal terms for two statistically most significant frequencies

HST-model	Metric / Value		Improvement (%)
optimal model	R^2	0.99	
	RMSE [*mm*]	1.01	
	SNR	18.40	
extended model-1.iteration	R^2	0.99	0%
$f_1 = 0.0018$	*RMSE* [*mm*]	0.96	5.0%
	SNR	18.84	2.4%
extended model-2.iteration	R^2	0.99	0%
$f_2 = 0.0023$	*RMSE* [*mm*]	0.88	8.3%
	SNR	19.66	4.4%

Abbreviations: HST, hydrostatic-season-time; RMSE, root mean square error; SNR, signal-to-noise ratio.

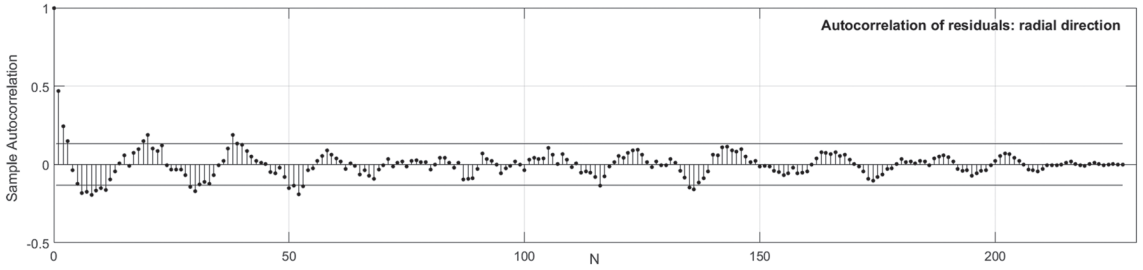

FIGURE 15 Autocorrelation of residuals after the inclusion of two additional periodicities into the optimal hydrostatic-season-time-model

5 | CONCLUSIONS

The empirical HST-model has been widely used for the analysis of displacement measurements, captured by different types of sensors, primarily on concrete dams. The residual time series, resulting after adopting an optimal HST-model for the data, can still expose underlying periodicities. In order to fulfill the preassumption of the regression analysis, and to assure a reliable estimate of model parameters, the deterministic patterns in residual time series should be analysed and extracted.

The displacements at the highest points of pendulum systems for any concrete dam are strongly influenced by the thermal effect. In the presented case study, there were two relative fast fillings in the reservoir for the analysed period that additionally influence the temperature variations in the dam body (at the highest levels). Therefore, the use of only

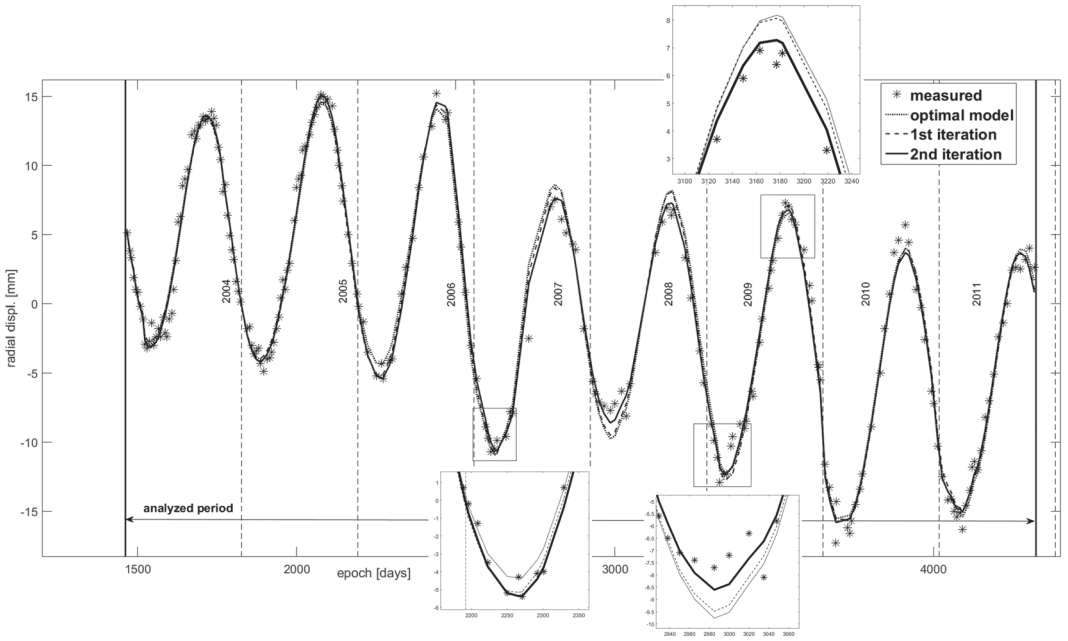

FIGURE 16 Comparison of measured and estimated displacements for the optimal and extended hydrostatic-season-time-model (1st and 2nd iteration)

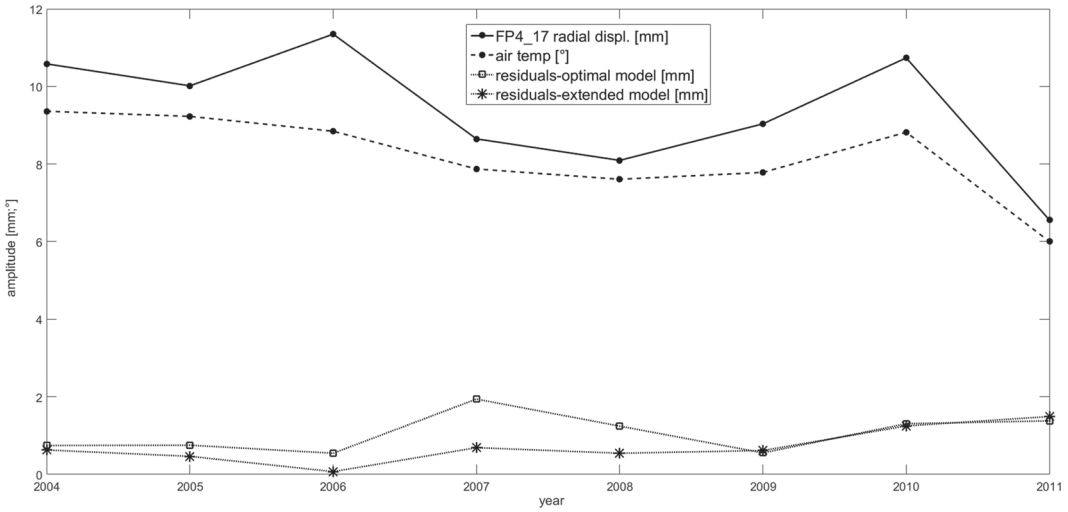

FIGURE 17 Annual amplitudes for air temperature, radial displacements, and residuals for an optimal and extended hydrostatic-season-time-model

one sinusoidal term with 1 year period to represent the temperature effect in the optimal HST-model may not be the best solution in the presented case study.

The main intent of the research work is to estimate—presumed nonannual—underlying periodicities in residual time series after adopting an optimal HST-model, their statistical significance, and their possible correlation to underlying periodicities in measurement time series of influential effects (water level and temperature) on the dam, and to assess their contribution in the minimisation of the residuals, in an iterative manner. Because the measurement data were captured manually, with an uneven time interval, except for the air temperature, the LSNP frequency method was used to analyse the frequencies of underlying periodicities.

The LSNP of time series of measured displacements detects and confirms the annual frequency as the statistically most significant. The periodicity is substantiated by a strong influence of the temperature, which follows an annual period, which is a well-known fact for concrete dams. A further frequency, detected as statistically highly significant at the 99.99% confidence level, corresponds to the period of 7 days and is interpreted as the time interval that appears most frequently

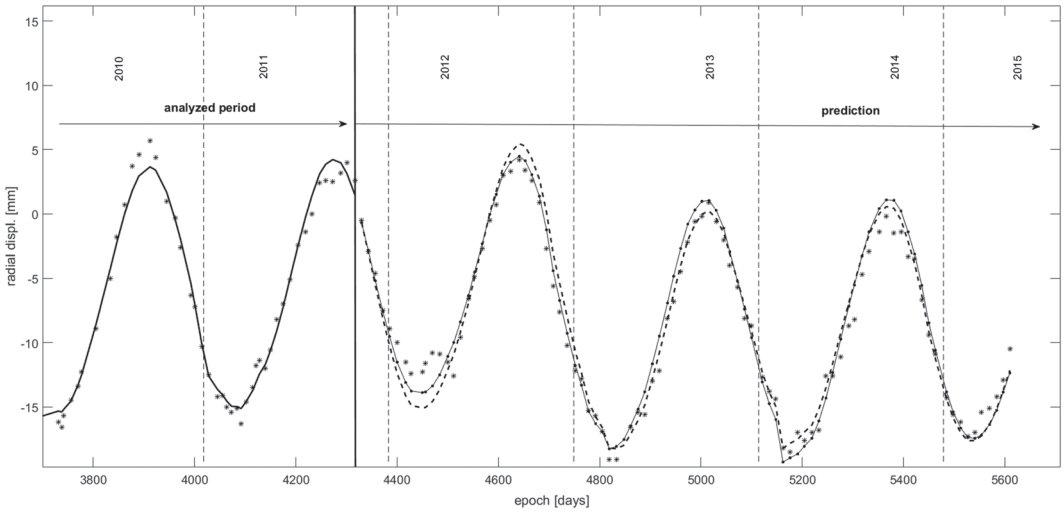

FIGURE 18 Predictions for an optimal (solid line with dots) and extended hydrostatic-season-time-model (dashed line)

in unevenly spaced data for all time series. Such effects are discussed in VanderPlas,[29] presented on an astronomical case study. Also in our case study, the spectral analysis of available different types of unevenly spaced data with sufficiently high sampling rates confirms this. The authors would like to stress that by adopting spectral analysis techniques for engineering purposes, the detected significant frequencies should be analysed for their possible correlation with the sampling intervals first.

After adopting the optimal HST-model, which involves modelling of the annual period, the LSNP is used to analyse residual time series in an iterative process. Namely, the frequency power spectrum detects statistically significant signals in relation to the background noise. A low frequency of 0.0018 per day, corresponding to the period of 1.5 years, and a low frequency of 0.0023 per day, corresponding to the period of 1.2 years, were detected as significant at the 90% and 99% confidence level in residual time series, in the first and second iteration, respectively. Adding additional sinusoidal terms for these two frequencies to the optimal HST-model contributes slightly to the improvement of the model error metrics and to the reduction of the residuals and their correlation in time domain. The extended HST-model shows predominantly an improved modelling of the changes in displacement amplitudes (Figure 17). Namely, in radial direction, the influence of the temperature is more significant, and the changes in temperature amplitudes influence directly the amplitudes of measured displacements, which are not directly modeled in the HST-model. Because the maximal improvements after adopting the extended HST-model amount up to 1.2 mm at the amplitudes of approximately annual periodicity, the extended model presents predominantly the statistical improvement of the optimal HST-model and does not influence the data interpretation and safety assessment with decision-making for the analysed pendulum reading station.

In order to utilise fully the potential of spectral analysis, the proposed methodology should be adopted for all reading stations of eight pendulum systems to examine whether some part of the dam exposes similar statistically significant frequencies. In this case, further attempts for their physical interpretation should be conducted.

ACKNOWLEDGEMENTS

The authors wish to acknowledge the hydropower company EDIA Empresa de Desenvolvimento e Infraestruturas do Alqueva, S.A., for providing the data available for the numerical evaluations in this paper and for a publication allowance.

ORCID

Sonja Gamse https://orcid.org/0000-0001-7032-7680

REFERENCES

1. Salazar F, Toledo M. Á, Oñate E, Morán R. An empirical comparison of machine learning techniques for dam behaviour modelling. *Struct Saf*. 2015;56:9-17. https://doi.org/10.1016/j.strusafe.2015.05.001
2. Mata J, Leitão N, Tavares de Castro A, Sá da Costa J. Construction of decision rules for early detection of a developing concrete arch dam failure scenario. A discriminant approach. *Comput Struct*. 2014b;142:45-53. https://doi.org/10.1016/j.compstruc.2014.07.002

3. Swiss Committee on Dams. Methods of analysis for the prediction and the verification of dam behaviour. Montreal. ICOLD; 2003: 73–110.
4. Gamse S, Oberguggenberger M. Assessment of long-term coordinate time series using hydrostatic-season-time model for rock-fill embankment dam. *Struct Control Health Monit*. 2017;24(1):e1859. https://doi.org/10.1002/stc.1859
5. Li F, Wang Z, Liu G. Towards an error correction model for dam monitoring data analysis based on cointegration theory. *Struct Saf*. 2013;43:12-20. https://doi.org/10.1016/j.strusafe.2013.02.005
6. Mata J, Tavares de Castro A, Sá da Costa J. Constructing statistical models for arch dam deformation. *Struct Control Health Monit*. 2014;21:423-437. https://doi.org/10.1002/stc.1575
7. Yu H, Wu Z, Bao T, Zhang L. Multivariate analysis in dam monitoring data with PCA. *Sci China Technol Sci*. 2010;53(4):1088-1097. https://doi.org/10.1007/s11431-010-0060-1
8. Salazar F, Morán R, Toledo M. Á, Oñate E. Data-based models for the prediction of dam behaviour: A review and some methodological considerations. *Arch Comput Method E*. 2017;24(1):1-21. https://doi.org/10.1007/s11831-015-9157-9
9. Mata J, Tavares de Castro A, Sá da Costa J. Time-frequency analysis for concrete dam safety control: Correlation between the daily variation of structural response and air temperature. *Eng Struct*. 2013;48:658-665. https://doi.org/10.1016/j.engstruct.2012.12.013
10. Lomb NR. Least-squares frequency analysis of unequally spaced data. *Astrophys Space Sci*. 1976;39:447-462. https://doi.org/10.1007/BF00648343
11. Vaníček P. Approximate spectral analysis by least-squares fit—Successive spectral analysis. *Astrophys Space Sci*. 1969:387-391. https://doi.org/10.1007/BF00651344
12. Vaníček P. Further development and properties of the spectral analysis by least squares. *Astrophys Space Sci*. 1971;12:10-33. https://doi.org/10.1007/BF00656134
13. Gamse S, Henriques MJ, Oberguggenberger M. Assessment of long term pendulum and geodetic observations on a concrete arch dam. In: 3rd Joint International Symposium on Deformation Monitoring; 2016; Vienna. https://www.fig.net/resources/proceedings/2016/2016_03_jisdm_pdf/nonreviewed/JISDM_2016_submission_46.pdf
14. Willm G, Beaujoint N. Les méthodes de surveillance des barrages au service de la production hydraulique dElectricité de France-Problèmes ancients et solutions nouvelles. In: 9th ICOLD Congress; Istanbul. 1967:529-550. q34-R30.
15. Montgomery DC, Runger GC. *Applied Statistics and Probability for Engineers*. New York: John Wiley & Sons Inc; 1994.
16. Farrar DE, Glauber RR. Multicollinearity in regression analysis: The problem revisited. *Rev Econ Stat*. 1967;49(1):92-107. https://doi.org/10.2307/1937887
17. Montgomery DC, Peck EA, Vining GG. *Introduction to Linear Regression Analysis*. 5th ed. Hoboken, New Jersey: John Wiley & Sons Inc; 2012.
18. Yuen K. *Bayesian Methods for Structural Dynamics and Civil Engineering*. Singapore: John Wiley & Sons (Asia) Pte Ltd; 2010.
19. Schwarz G. Estimating the dimension of a model. *Ann Statist*. 1978;6(2):461-64.
20. Akaike H. A new look at the statistical model identification. *IEEE Trans Autom Control*. 1974;19(6):716-23.
21. Kaczmarek A, Kontny B. Identification of the noise model in the time series of GNSS stations coordinates using wavelet analysis. *Remote Sens*. 2018;10(10):1611. https://doi.org/10.3390/rs10101611
22. Nobakht-Ersi F, Gamse S, Sharifi MA. Identification of significant periodicities in daily GPS time series using least-squares spectral analysis. *Arab J Geosci*. 2016;9:493. https://doi.org/10.1007/s12517-016-2468-9
23. Erol B. Evaluation of high-precision sensors in structural monitoring. *Sensors*. 2010;10(12):10803-10827. https://doi.org/10.3390/s101210803
24. Zhang Q, Ma C, Meng X, et al. Galileo augmenting GPS single-frequency single-epoch precise positioning with baseline constrain for bridge dynamic monitoring. *Remote Sens*. 2019;11(4):438. https://doi.org/10.3390/rs11040438
25. Pytharouli SI, Stiros SC. Ladon dam (Greece) deformation and reservoir level fluctuations: Evidence for a causative relationship from the spectral analysis of ageodetic monitoring record. *Eng Struct*. 2005;27:361-370. https://doi.org/10.1016/j.engstruct.2004.10.012
26. Pytharouli SI, Stiros SC. Spectral analysis of unevenly spaced or discontinuous data using the normperiod code. *Comput Struct*. 2008;86(1–2):190-196. https://doi.org/10.1016/j.compstruc.2007.02.022
27. Scargle JD. Studies in astronomical time series analysis. II. Statistical aspects of spectral analysis of unevenly spaced data. *Astrophys J*. 1982;263:835-835.
28. Press WH, Rybicki GB. Fast algorithm for spectral analysis of unevenly sampled data. *Astrophys J*. 1989;338:277-280.
29. VanderPlas JT. Understanding the lomb-scargle periodogram. *Astrophys J Suppl S*. 2018;236(1). https://doi.org/10.3847/1538-4365/aab766
30. Press WH, Teukolsky SA, Vetterling WT, Flannery BP. *Numerical recipes in C. The Art of Scientific Computing*. 2nd ed.. Cambridge: Cambridge University Press; 1988–1992. https://www2.units.it/ipl/students_area/imm2/files/Numerical_Recipes.pdf
31. Baluev RV. Assessing the statistical significance of periodogram peaks. *Mon Not R Astron Soc*. 2008;385(3):1279-1285. https://doi.org/10.1111/j.1365-2966.2008.12689.x
32. Zhou W, Sornette S. Statistical significance of periodicity and log-periodicity with heavy-tailed correlated noise. *Int J Mod Phys C*. 2002;13(2):137-169. https://doi.org/10.1142/S0129183102003024
33. Tavares de Castro A, Henriques MJ. Monitoring planimetric displacements in concrete dams. In: 13th FIG Symposium on Deformation Measurement and Analysis LNEC; 2008; Lisbon, Portugal. Available online: https://www.fig.net/resources/proceedings/2008/lisbon_2008_comm6/papers/pas05/pas05_02_tavaresdecastro_mc127.pdf
34. Laboratório Nacional de Engenharia Civil - LNEC. Observation plan of Alqueva scheme. Dam, foundation, surrounding rock mass, reservoir and appurtenant works (in Portuguese). Internal report, Lisbon, LNEC; 1997. n. 244/97-NO/DB

35. RSB. Regulation for safety of dams. (in Portuguese). Decree-law n. 344/2007.
36. Laboratório Nacional de Engenharia Civil - LNEC. Alqueva scheme: Preliminary plan of the geodetic observation system (in Portuguese). Internal report, Lisbon, LNEC; 2000. n. NT 19/2000-NMG/DB
37. Laboratório Nacional de Engenharia Civil - LNEC. Alqueva scheme: Note on the Geodetic Observation System. (in Portuguese). Internal report, Lisbon, LNEC; 2001a. n. NT 01/2001-NMG/DB
38. Laboratório Nacional de Engenharia Civil - LNEC. Alqueva scheme: The precision traverse on the crest of the dam. (in Portuguese). Internal report, Lisbon, LNEC; 2001b. n. NT 11/2001-NMG/DB
39. Jung IS, Berges M, Garrett JH, Poczos B. Exploration and evaluation of AR, MPCA and KL anomaly detection techniques to embankment dam piezometer data. *Adv Eng Inform*. 2015;29(4):902-917. https://doi.org/10.1016/j.aei.2015.10.002
40. Salazar F, Toledo M. Á, González JM, Oñate E. Early detection of anomalies in dam performance: A methodology based on boosted regression trees. *Struct Control Health Monit*. 2017;24(11):e2012. https://doi.org/10.1002/stc.2012
41. Koen C. The Nyquist frequency for irregularly spaced time-series: A calculation formula. *Mon Not R Astron Soc*. 2006;371(3):1390-1394. https://doi.org/10.1111/j.1365-2966.2006.10762.x

How to cite this article: Gamse S, Henriques MJ, Oberguggenberger M, Mata JT. Analysis of periodicities in long-term displacement time series in concrete dams. *Struct Control Health Monit*. 2019;e2477. https://doi.org/10.1002/stc.2477